



Performance of the IRI-2016 over Santa Maria, a Brazilian low-latitude station located in the central region of the South American Magnetic Anomaly (SAMA)

Juliano Moro^{1,2}, Jiyao Xu¹, Clezio Marcos Denardini³, Laysa Cristina Araújo Resende^{1,3}, Régia Pereira Silva³, Sony Su Chen³, Giorgio Arlan da Silva Picanço³, Liu Zhengkuan¹, Hui Li¹, Chunxiao Yan¹, Chi Wang¹, and Nelson Jorge Schuch²

¹State Key Laboratory of Space Weather – NSSC/CAS, Beijing, China

²Southern Regional Space Research Center – CRCRS/COCRE/INPE-MCTIC, Santa Maria, Brazil

³DIDAE: National Institute for Space Research – INPE/MCTIC, São José dos Campos, Brazil

Correspondence: Juliano Moro (juliano.moro@inpe.br)

Received: 26 August 2019 – Discussion started: 10 September 2019

Revised: 28 February 2020 – Accepted: 10 March 2020 – Published: 6 April 2020

Abstract. In this work we analyze the ionograms obtained by the recent digisonde installed in Santa Maria (29.7° S, 53.7° W, dip angle = -37°), Brazil, to calculate the monthly averages of the F2 layer critical frequency (f_oF2), its peak height ($hmF2$), and the E-region critical frequency (f_oE) acquired during geomagnetically quiet days from September 2017 to August 2018. The monthly averages are compared to the 2016 version of the International Reference Ionosphere (IRI) model predictions in order to study its performance close to the center of the South America Magnetic Anomaly (SAMA), which is a region particularly important for high-frequency (HF) ground-to-satellite navigation signals. The f_oF2 estimated with the Consultative Committee International Radio (CCIR) and International Union of Radio Science (URSI) options makes good predictions throughout the year, whereas, for $hmF2$, it is recommended to use the SHU-2015 option instead of the other available options (AMTB2013 and BSE-1979). The IRI-2016 model outputs for f_oE and the observations presented very good agreement.

1 Introduction

The growing importance of space technologies through satellites for a large variety of applications such as science, Earth observation, meteorology, communications, security, and defense puts forward the need to improve our ability of iono-

spheric modeling. For instance, the drag force on satellites in low-Earth orbit (LEO, generally defined as an orbit below an altitude of approximately 2000 km) increases when the solar activity is at its greatest over the 11-year solar cycle, which may cause uncontrolled re-entry and degrade the predictions of satellite positions (Horne et al., 2013). During space weather conditions as defined by Denardini et al. (2016), elevated flux levels of high energetic particles may precipitate in the ionosphere in regions of anomalously weak geomagnetic field strength such as the South America Magnetic Anomaly (SAMA). Besides enhancing the ionization distribution and conductivities (Moro et al., 2012, 2013), the energetic particles create high background counts which render satellite sensors unusable in this region (Schuch et al., 2019; Heirtzler, 2002). Operators who control satellites in LEO may need to know with a high degree of accuracy when and where to turn satellites on and off to minimize the risk of detector saturation (Jones et al., 2017). Ionospheric modeling is also important for ground assets since it is essential to predict the ionospheric behavior for successful radio communication. Since drastic ionospheric variations can affect the performance of radio-based systems, such prediction may identify the periods, the path regions, and the sections of high-frequency bands that will allow or disrupt the use of the radio transmissions (Ezquer et al., 2008).

One of the most widely used ionospheric models is the International Reference Ionosphere (IRI), which became

the official International Standardization Organization (ISO) standard for the ionosphere in April 2014 (Bilitza et al., 2017). IRI is a joint project of the Committee on Space Research (COSPAR) and International Union of Space Science (URSI). It is derived from ionospheric observations collected by ground and in situ measurements such as the worldwide network of ionosondes, incoherent scatter radars, several compilations of rocket measurements, and satellite data. The model describes monthly averages of the electron density, electron and ion temperature, total electron content (TEC), and ion composition as a function of height, location, and local time. Several major milestone editions of IRI have been released by the IRI Working Group since the 1970s in order to constantly revise the model to keep it as up to date and accurate as possible (Rawer et al., 1978a, b, 1981; Bilitza, 1990, 2001; Bilitza and Rawer, 1996; Bilitza and Reinisch, 2008; Bilitza et al., 2014, 2017). The latest version is known as IRI-2016 and has important improvements over the 2012 and 2007 versions (IRI-2012 and IRI-2007, respectively). The most important update is the inclusion of two new model options for the F2 layer peak height, $hmF2$. These two options allow the users to model the $hmF2$ directly and no longer depend on the propagation factor $M3000F2$ described by Bilitza et al. (1979). Besides, IRI-2016 has a better representation of topside ion densities during very low and high solar activities. The details about the IRI model are available on the following home page: <http://irirmodel.org/> (last access: 12 August 2019).

Among several parameters, IRI can predict the F2 layer critical frequency ($foF2$), $hmF2$, and the E-region critical frequency (foE) for a given time and location. The correct understanding of these parameters is particularly important for space technologies. The critical frequencies are two key parameters when calculating the electron densities of the ionosphere at F2 ($NmF2$) and E-region heights. Moreover, $foF2$ is related to the maximum usable frequency for the radio waves reflection and TEC that is significant for the phase delay of high-frequency (HF) ground-to-satellite navigation signals (Fuller-Rowell et al., 2000). On the other hand, $hmF2$ receives much of the attention since it gives the highest stratification of the upper ionosphere.

In the literature, several papers have reported many comparative studies around the globe between the ionospheric parameters measured by ionosondes and different versions of the IRI to study its performance. In South America, Ezquer et al. (2008) analyzed $NmF2$ over Tucumán (26.9° S, 66.4° W, dip angle = -26°), Argentina, during the low and high solar activity years 1965 and 1970, respectively, and the moderate solar activity years 1967 and 1972. Bertoni et al. (2006) used $foF2$ and $hmF2$ measured by two digital ionosondes installed at two Brazilian low-latitude stations in July 2003, October 2003, January 2004, and April 2004. They compared the data collected in Palmas (10.1° S, 48.2° W, dip angle = -12°) and São José dos Campos (23.2° S, 45.8° W, dip angle = -33°) with the IRI-2001 predictions. Batista and

Abdu (2004) compared the parameters $foF2$, $hmF2$, and B_0 measured by two digital ionosondes over São Luís (2.6° S, 44.2° W, dip angle = -4.3°, magnetic equator) and Cachoeira Paulista (22.7° S, 45° W, dip angle = -33.5°, close to the southern crest of the equatorial ionization anomaly – EIA) with the IRI-2007 for high and low solar activity periods. Moro et al. (2016) tested the influence of IRI-2007 in deriving the conductivity profiles and electric fields in the Brazilian equatorial region. In Africa, Oyekola and Fagundes (2012) compared $foF2$, $hmF2$, and propagation factor ($M3000F2$) recorded near the dip-equator in Ouagadougou, Burkina Faso (12° N, 1.8° W; dip angle = 2.9°) with IRI-2007 during low (1987) and high (1990) solar activity, and undisturbed conditions for four different seasons. In Europe, Maltseva and Poltavsky (2009) investigated several aspects of the IRI accuracy and efficiency for long-term prediction of the $foF2$ and the maximum usable frequencies (MUF) using the storm-time correction option, TEC, and the maximum observable frequency (MOF) for the year 2005. In China, Zhao et al. (2017) used $hmF2$ data derived by ionosondes at Mohe, Beijing, Wuhan, and Sanya from 2007 to 2016 to assess the performance of the three options for the IRI $hmF2$, while Liu et al. (2019) used $foF2$ measured over four stations in China (covering from 49.4 to 23.2° N) from January 2008 to October 2016 to test IRI $foF2$. The aforementioned studies show that the ionospheric parameters predicted by the IRI model differed from the ionosonde data at a different location. Generally, IRI overestimates the ionospheric parameters at the magnetic equator and underestimates at EIA crests.

The aim of this work is to use the critical frequencies $foF2$ and foE and the height $hmF2$ measured by a recent 4D digisonde portable sounder (DPS-4D) installed in Santa Maria (29° S, 54° W, dip angle = -37°), Brazil, to test the performance of the IRI-2016 in the low-latitude ionosphere situated close to the center of the SAMA. The Santa Maria digisonde (SMK29) is supported by the Space Weather Monitoring Meridian Project of China (Wang, 2010), the Brazilian Study and Monitoring of Space Weather (Embrace) Program from the Brazilian National Institute for Space Research (INPE/MCTIC), and the Federal University of Santa Maria (UFSM). Notice that there are very few ionospheric sounders operating in real-time in the low- and mid-latitudes in South America, and SMK29 fills a gap of ionospheric sounding between Cachoeira Paulista station and Port Stanley station (51.6° S, 57.9° W, dip angle = -49.8°), Argentina. Therefore, validating the IRI-2016 in a region under the influence of the SAMA is particularly important for HF communication and radio-based space systems as described before, as is the contribution of the IRI Working Group in evaluating the efficacy of the model in the low-latitude Brazilian region.

Table 1. The 27 d averaged values of F10.7, sunspot number, and the number of quiet-days from September 2017 to August 2018 considered in this work.

Year	Month	F10.7	Sunspot number	Amount of quiet days
2017	Sep	80.1	18	11
	Oct	72.1	8	18
	Nov	70.3	8	17
	Dec	69.4	9	21
2018	Jan	67.7	6	24
	Feb	70.4	12	20
	Mar	67.6	1	21
	Apr	70.3	10	24
	May	70.7	7	22
	Jun	74.5	16	23
	Jul	74.7	12	26
	Aug	71.2	1	21
Total				248

2 Observed data, modeling, and method of analysis

The SMK29 is set to transmit radio waves continuously into the ionosphere from 1 MHz and increases the frequency up to 20 MHz with the sweep rate of 25 kHz for each round. The train of echoes to form an ionogram is transmitted and received with a 5 min temporal resolution. All recorded ionograms are initially auto-scaled by the Automatic Real-Time Ionogram Scaler with True Height (ARTIST). Then, the observed *foF2*, *foE*, and *hmF2* parameters are deduced from manually scaled ionograms with help of the digisonde ionogram data visualization and editing tool SAO-Explorer, developed by the Center for Atmospheric Research, University of Lowell Massachusetts.

Data used in this work were collected on geomagnetically quiet days ($\sum Kp \leq 24$, where $\sum Kp$ is the sum of the eight 3 h *Kp* indices for the day) from September 2017 to August 2018. The period is characterized by a very low level of solar and magnetic activity. The 27 d averaged values of the F10.7, the sunspot numbers, and the numbers of monthly quiet data used in this work are shown in Table 1. The average of the solar emission at a wavelength of 10.7 cm from September 2017 to August 2018 is only $(71.6 \pm 3.5) \times 10^{-22} \text{ W m}^{-2} \text{ Hz}^{-1}$, and the sunspot numbers range from 1 to 18, characterizing the period of low solar activity.

Monthly average values of the observed *foF2*, *foE*, and *hmF2* parameters are calculated from the daily hourly values. The IRI-2016 predictions of *foF2*, *foE*, and *hmF2* are computed for the same geophysical conditions to compare with the observational data and to evaluate the discrepancies and goodness of the model. The relative deviation (R_D) of the predicted values concerning the observed values for mod-

eling the *foF2* using the Consultative Committee on International Radio (CCIR) coefficient (CCIR, 1967) were computed through Eq. (1).

$$foF2_{CCIR-RD} = \left(\frac{foF2_{CCIR} - foF2_{Observed}}{foF2_{Observed}} \right) \times 100\% \quad (1)$$

The term $foF2_{CCIR}$ stands for the monthly average of the *foF2* modeled by the CCIR sub-routine, while the term $foF2_{Observed}$ is the monthly average of *foF2* measured by the SMK29. Besides the comparison between the observed *foF2* with CCIR, the sub-routine URSI (Rush et al., 1989) is also tested and, therefore, Eq. (1) is also used considering $foF2_{URSI}$ instead of $foF2_{CCIR}$. The *foF2* storm model (Araujo-Pradere et al., 2002) was turned off in the IRI-2016 options since we are interested in the quiet-time conditions. The R_D is also evaluated for *hmF2* and *foE* using Eq. (1). For *hmF2*, the comparison is made using the three currently available options for determining IRI *hmF2*: AMTB2013 (Altadill et al., 2013), SHU-2015 (Shubin, 2015), and BSE-1979 (Bilitza et al., 1979), called AMTB, SHU, and BSE, respectively, hereafter. The AMTB model is based on ionospheric data deduced from ionograms recorded by 26 digisondes embracing latitudes from 65° N to 52° S and the longitude sector from 120° W to 170° E. The data cover different levels of solar activity from 1998 to 2006. The spherical harmonic technique was applied in AMTB to model the quiet pattern of the *hmF2* at a global scale. The SHU model is based on the ionospheric radio-occultation data collected by CHAMP (from 2001 to 2008), GRACE (from 2007 to 2011), and COSMIC (from 2006 to 2012) satellite missions and ionospheric sounding data collected by 62 digisondes from 1987 to 2012. SHU uses the spherical harmonics decomposition to model *hmF2*. Finally, the older BSE uses the correlation between *hmF2* and propagation factor $M3000F2$, which in turn is defined by the ratio between the highest frequency that, refracted by the ionosphere, can be detected at a distance of 3000 km ($M3000$) and *foF2*. At last, the *foE* comparison is made using IRI *foE* developed by Kouris and Muggleton (1973a, b) for CCIR (1973) with a modified zenith angle introduced by Rawer and Bilitza (1990) to improve the nighttime variations. Finally, to evaluate the performance of IRI-2016, a correlation analysis is performed between the modeled parameters and the observational data.

In some cases, the results are discussed considering the seasonal differences between the observed and modeled parameters. Each season is composed of three months as follows: December solstice (November, December, and January), March equinox (February, March, and April), June solstice (May, June, and July), and September equinox (August, September, and October). The local time (LT) in Santa Maria is defined as the universal time (UT) less three hours ($LT = UT - 3 \text{ h}$). Finally, since the focus of this work is to analyze the IRI-2016 predictions, the reader can find the complete study about the variabilities of the F2 and E layer pa-

parameters over Santa Maria during the period analyzed in the recent work by Moro et al. (2019).

3 Results

3.1 Performance of IRI in the F-region parameters

The contour plots of the monthly averaged f_oF2 (in MHz) observed and modeled by CCIR and URSI sub-routines, and the R_D (in percent) versus universal time (UT, vertical axis) and months (from September 2017 to August 2018, horizontal axis) are shown in Fig. 1. The f_oF2 values are represented by the color-coded bar on the right-hand side of panels a–c and vary from 1 to 12 MHz. The R_D in panels d–e ranges by $\pm 50\%$.

During the whole year analyzed the sunrise time varied from 09:15 to 10:30 UT, while the sunset took place between 20:43 and 23:30 UT over Santa Maria. The observed averaged f_oF2 values depicted in Fig. 1a show a diurnal variation pattern, with the highest values occurring during daytime hours (13:00–22:00 UT) and the lowest values occurring during pre-sunrise hours (around 08:00 UT). We attribute these values to the daytime dynamics over Santa Maria, e.g., photoionization and neutral atmospheric dynamics (Moro et al., 2019; Abdu and Brum, 2009). The highest values of around 11 MHz are observed between 17:00 and 20:00 UT from September to March, evidencing the seasonal trends. The lowest values of around 1.5 MHz occur between 07:00 and 09:00 UT during the June solstice months. Regarding the CCIR prediction shown in Fig. 1b and URSI predictions in Fig. 1c, f_oF2_{CCIR} and f_oF2_{URSI} , respectively, very similar diurnal and seasonal variation patterns to those seen in the observed values are observed. However, a first look at the $f_oF2_{CCIR-RD}$ in Fig. 1d and $f_oF2_{URSI-RD}$ in Fig. 1e reveals that the coefficient outputs grossly underestimate or overestimate the f_oF2 in some hours and months, as indicated below.

The $f_oF2_{CCIR-RD}$ in Fig. 1d ranges from -20% (underestimation) to 50% (overestimation). The higher underestimations are observed in September and October from 09:00 to 16:00 UT, and later from November to February between 20:00 and 22:30 UT. There is also an underestimation of 20% from April to August at around 10:00 UT. On the other hand, the overestimations are most significant during nighttime hours in almost all months from 23:00 to 08:00 UT. The $f_oF2_{URSI-RD}$ varies from -15% to more than 50% . The most negative deviations are observed only in two small portions of the contour plot in Fig. 1e, which is around 21:00 UT in October, and from 18:00 to 22:00 UT in December. However, significant positive deviations higher than 50% are seen around 09:00 UT from March to July, and in the nighttime hours around 23:00 UT from February to April. From these results, it seems that the URSI (CCIR) sub-routine overestimates (underestimates) f_oF2 more than the CCIR (URSI).

A more detailed analysis has to be performed to further investigate the level of reliability of each IRI sub-routine. Since the data are not significantly drawn from a normally distributed population at the 0.05 % level, the quantitative estimate can be achieved by analyzing the statistical relationship between IRI f_oF2 and observed values using the Spearman correlation coefficient (r). The significance of the calculated r value is examined with a confidence level of 95 % between the hourly values modeled and observed data. The scatter plots of modeled IRI f_oF2 using CCIR and URSI coefficients versus the observational data are shown in Fig. 2. The results of the calculated r are 0.97 for both IRI coefficients. An almost perfect positive correlation is shown.

The contour plots of the monthly averaged $hmF2$ (in km) observed by the SMK29 and modeled by AMTB, SHU, and BSE sub-routines and the R_D (in percent) versus universal time (UT, vertical axis) and month (from September 2017 to August 2018, horizontal axis) are shown in Fig. 3. The color-coded bar on the right-hand side of panels a–d represent $hmF2$ ranging from 180 to 360 km. In panels e–g, the color-coded bar refers to the R_D and ranges $\pm 50\%$ for the three plots. The observed $hmF2$ values in Fig. 3a show that the F2-layer is higher during nighttime hours, achieving 340 km from September to December from 01:00 UT to around 03:00 UT. There is also more intense $hmF2$ values between 300 and 320 km during the September equinox and December solstice months from 12:00 to 18:00 UT. The daytime average values in the March equinox and June solstice months are usually below 240 km. The more intense values during nighttime in all months and in the daytime during the September equinox and December solstice months are quite well represented by the AMTB in Fig. 3b, SHU in Fig. 3c, and BSE in Fig. 3d as well as the low values during the daytime from the March equinox and June solstice months. Although there are similarities, IRI-2016 predictions have some different aspects, as shown by the $hmF2_{AMTB-RD}$ in Fig. 3e, $hmF2_{SHU-RD}$ in Fig. 3f, and $hmF2_{BSE-RD}$ in Fig. 3g. A visual comparative analysis shows that the SHU agrees better with the observations since the RD encompasses, in general, $\pm 10\%$ most of the time. The same is not true for AMTB and BSE predictions.

The $hmF2_{AMTB-RD}$ ranges from -10% to 43% . The main differences are related to the overestimation of $hmF2$ most of the time in September and October and from March to August as represented by the hottest color of the palette. It differs in particular near the sunrise period from 07:00 to 11:00 UT in the June equinox. The $hmF2_{SHU-RD}$ varies from -20% to 20% . In general, the SHU outputs differ only $\pm 10\%$ from the observation results, revealing very good agreement with the observations. Regarding $hmF2_{BSE-RD}$, it ranges from -24% to 20% . There are some small periods near sunrise (sunset) in which $hmF2$ is overestimated (underestimated), but in general, BSE also represents the observations well. As shown by the results presented in Fig. 3, SHU and BSE perform better than AMTB in modeling $hmF2$. This

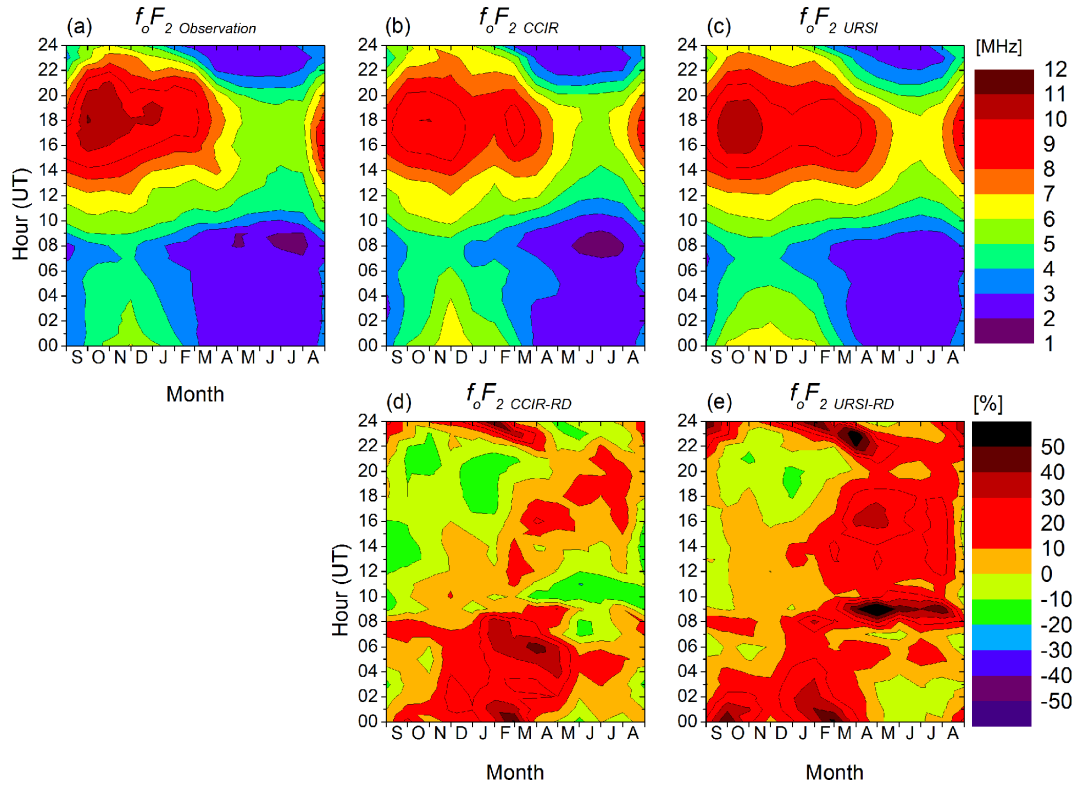


Figure 1. Contour plot of the monthly averaged f_oF_2 (a) measured by the Santa Maria digisonde (SMK29), provided by (b) CCIR and (c) URSI coefficients. The respective relative deviation (R_D) in percent is placed in the lower panels for (d) CCIR and (e) URSI.

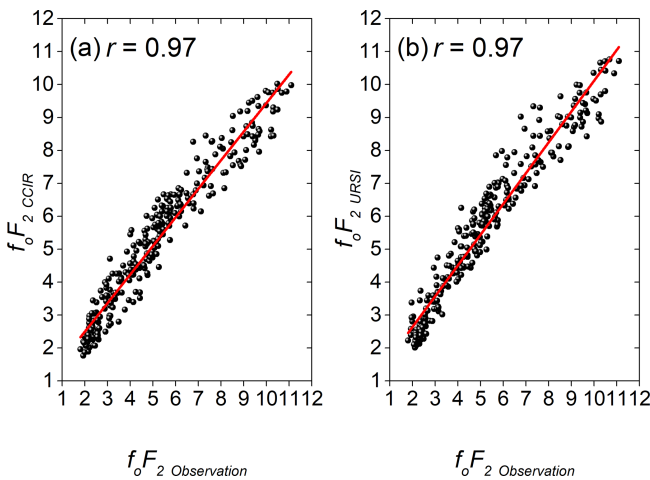


Figure 2. Scatter plots depicting the comparison between (a) $f_oF_2_{CCIR}$ and (b) $f_oF_2_{URSI}$ versus $f_oF_2_{Observation}$.

result is also confirmed by the statistical relationship shown by the Spearman r values shown in Fig. 4. Modeling the hmF_2 with the SHU coefficients presents the best scenario with the $r = 0.86$, as shown in Fig. 4b. Despite the AMTB in Fig. 4a presenting the lower correlation ($r = 0.72$), it is important to note that it is still significant.

3.2 Performance of IRI f_oE

The contour plots of the monthly averaged f_oE (in MHz) observed by the SMK29 and modeled by IRI-2016 and the estimated R_D (in percent) versus universal time (UT, vertical axis) and month (from September 2017 to August 2018, horizontal axis) are shown in Fig. 5. The f_oE values are represented by the color-coded bar on the right-hand side, ranging from 1 to 3.5 MHz for the critical frequency in panels a–b, and $\pm 20\%$ for the R_D in panel c.

The observed f_oE in Fig. 5a shows a regular diurnal variation, increasing from sunrise to a peak in the afternoon to around 3.5 MHz, and falling until sunset. The low electron density at night makes it difficult to detect the E region by the digisonde. The most intense values of around 3.5 MHz are seen during the September equinox and December solstice months. The agreement between IRI f_oE and observations is very good, as shown in Fig. 5b. The maxima values seen in IRI occur for longer than in the observations, however. They are shifted two months (April and May) and start earlier (July). The f_oE_{IRI-RD} in Fig. 5c are positive (overestimation) up to 5% only, confirming the good IRI-2016 performance in modeling f_oE almost all the time over Santa Maria. There are some considerable differences in a short time in the sunrise and sunset hours. These are critical periods which may be caused by distortions in the E-region traces due to horizontal

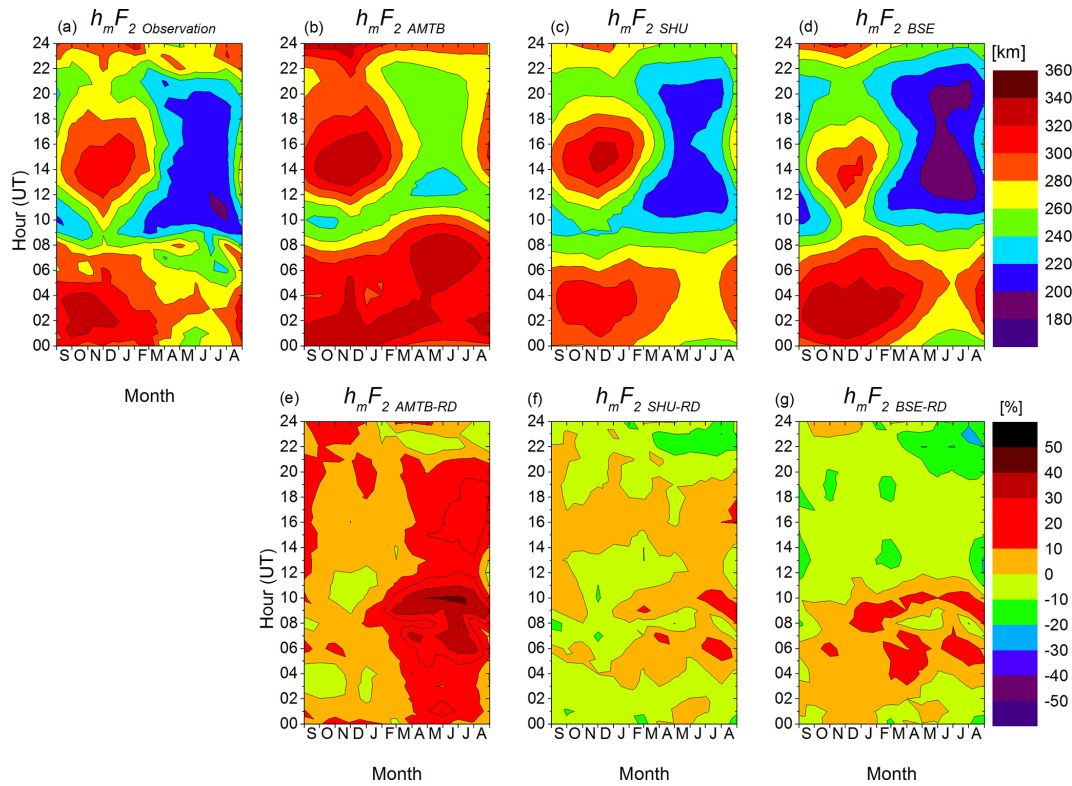


Figure 3. Contour plot of the monthly averaged $h_m F_2$ (a) measured by the Santa Maria digisonde (SMK29), provided by (b) AMTB, (c) SHU, and (d) BSE coefficients. The respective relative deviation (R_D) in percent is placed in the lower panels for (e) AMTB, (f) SHU, and (g) BSE.

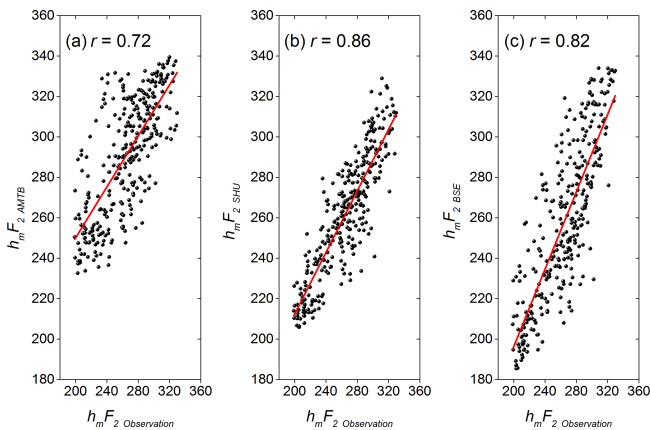


Figure 4. Scatter plots depicting the comparison between (a) $h_m F_2$ AMTB, (b) $h_m F_2$ SHU, and (c) $h_m F_2$ BSE versus $h_m F_2$ Observation.

gradients in the ionosphere, making it difficult to model with IRI, as can be expected by the users. The r value obtained between the modeled and observed values is the highest in this work, showing a very strong positive correlation, as shown in Fig. 6.

4 Discussion

The focus of this work is to use the foF_2 , foE , and $h_m F_2$ measured by the recent digisonde installed in Santa Maria, Brazil, to test the performance of the IRI-2016 in the low-latitude ionosphere situated close to the center of the SAMA during the geomagnetically quiet days from September 2017 to August 2018. The results presented in Figs. 1 and 2 show that the foF_2 predictions obtained with CCIR and URSI coefficients are very similar in a month-by-month analysis. However, CCIR (URSI) underestimates (overestimates) foF_2 during specific nighttime hours. When the whole period of data is considered, both coefficients gave r equal to 0.97. The correlation is an indication that the model accurately predicts the diurnal and seasonal trends of foF_2 over Santa Maria. In general, the IRI user may choose any sub-routine to model foF_2 .

The results obtained in this work closely follow the earlier work of Ezquer et al. (2008), who had compared the CCIR and URSI coefficients with the ionosonde data in Tucumán. They report that, in general, both coefficients give comparable values. However, they also report disagreements among predictions and measurements reaching values of R_D close to 50%. In the Brazilian sector, Batista and Abdu (2004) in a similar comparative study pointed out that the agreements between the URSI values and the observed foF_2 in São Luís

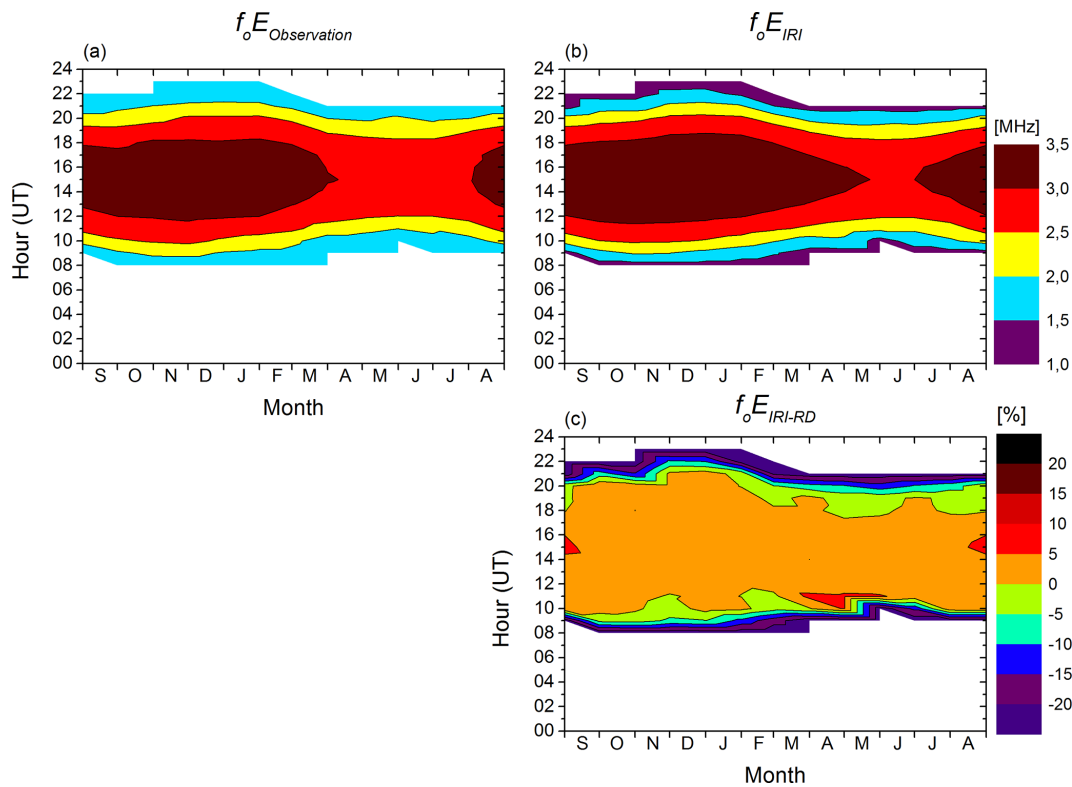


Figure 5. Contour plot of the monthly averaged f_oE (a) measured by the Santa Maria digisonde (SMK29), provided by (b) IRI, and (c) the relative deviation (R_D) in percent.

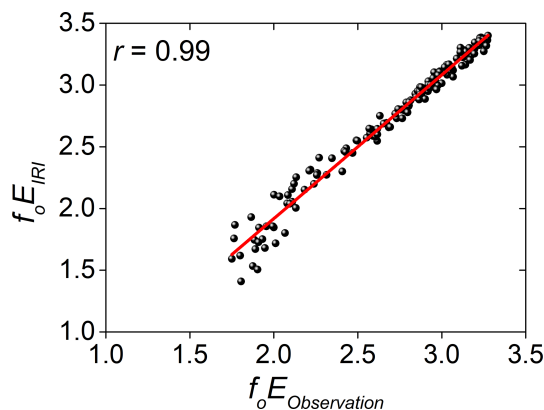


Figure 6. Scatter plot depicting the comparison between f_oE_{IRI} versus $f_oE_{Observation}$.

were always better as compared to the CCIR coefficients. They also showed that the f_oF2 after sunset is overestimated for the equatorial station of São Luís. It seems that over the Brazilian territory the right choice between CCIR and URSI in modeling f_oF2 depends on the location of the users. In the Brazilian equatorial region, CCIR performs better, while in the SAMA region there are no appreciable differences between both. In China, Liu et al. (2019) found that the CCIR

performs better than URSI during post-sunset under low solar activity or in the EIA region. For other times and outside the EIA region over China CCIR shows no large difference in performance as compared to URSI.

Figures 3 and 4 show that the SHU option for modeling the $hmF2$ performs better over Santa Maria, followed by BSE, and the AMTB is the worst. The r value of AMTB is 0.72, the lowest observed in the present study. It is even lower than the older BSE coefficient used in the previous versions of the IRI model. Overall, the AMTB (BSE) overestimated (underestimated) the observed values. Therefore, it is recommended to use the SHU option when modeling the $hmF2$ over Santa Maria. These results agree with the findings of Zhao et al. (2017), who also recommend the use of SHU option over China region when using IRI-2016 to model $hmF2$. Since this is the first evaluation of the three IRI $hmF2$ options in the Brazilian sector to the author’s knowledge, there is no comparison between our work with other Brazilian equatorial or low latitude regions, and this is suggested for a future study.

Finally, the comparative results presented in Figs. 5 and 6 show that the IRI-predicted f_oE values are in excellent agreement with observations in Santa Maria. The calculated r value is 0.99. The strong correlation may be explained by the fact that the E region ionization is subject to solar radiation control, and therefore IRI predicts the E region so-

lar ionization fairly accurately everywhere across the globe since there is no plasma transport in the E region.

5 Conclusions

The present work uses the f_oF2 , f_oE , and $hmF2$ parameters acquired by a recent digisonde installed in Santa Maria, Brazil, close to the center of the SAMA, to test the performance of the IRI-2016. Only data collected under geomagnetically quiet conditions from September 2017 to August 2018 are used to eliminate the effects of geomagnetic disturbances. Monthly average values of the observed ionospheric parameters are calculated from the daily hourly values and compared with the IRI-2016 predictions for the same geophysical conditions. The relative deviation (R_D) was computed using the CCIR and URSI coefficients to estimate the IRI f_oF2 performance. The IRI $hmF2$ predictions are evaluated using the R_D estimated using the three options AMTB, SHU, and BSE. The IRI f_oE performance is also tested. The main findings of the study are as follows:

- CCIR and URSI predictions represent the diurnal and seasonal variation patterns of the observed values. $f_oF2_{CCIR-RD}$ ranges from -20% (underestimation) to 50% (overestimation). The higher underestimations are observed in September and October from 09:00 to 16:00 UT, and later from November to February between 20:00 and 22:30 UT. There is also an underestimation of 20% from April to August at around 10:00 UT. The overestimations are most significant during nighttime hours during almost all months from 23:00 to 08:00 UT. The $f_oF2_{URSI-RD}$ varies from -15% to more than 50% . The most negative deviations are observed at around 21:00 UT in October, and from 18:00 to 22:00 UT in December. Significant positive deviations higher than 50% are seen at around 09:00 UT from March to July, and in the nighttime hours around 23:00 UT from February to April.
- SHU agrees better with the observations than AMTB and BSE for modeling $hmF2$. The $hmF2_{AMTB-RD}$ ranges from -10% to 43% . The main differences are related to the overestimation of $hmF2$ most of the time in September and October and from March to August. It differs in particular near the sunrise period from 07:00 to 11:00 UT in June equinox. The $hmF2_{SHU-RD}$ varies from -20% to 20% and, in general, differs by only $\pm 10\%$ from the observation. The results reveal very good agreement with the observations. $hmF2_{BSE-RD}$ ranges from -24% to 20% . There are some small periods near sunrise (sunset) in which $hmF2$ is overestimated (underestimated), but in general, BSE also represents the observations well.
- The agreement between IRI f_oE and observations is very high. However, the maxima values seen in IRI oc-

cur for longer than in the observations, as well as being shifted two months (April and May) and starting earlier (July). The f_oE_{IRI-RD} values are positive (overestimation) up to 5% only, confirming the good IRI-2016 performance in modeling f_oE almost all the time over Santa Maria, except for a short time in the sunrise and sunset hours.

As a general conclusion of this work, it is shown that both CCIR and URSI coefficients have high accuracy in predicting f_oF2 over Santa Maria. The same is true for IRI f_oE . However, it is recommended that the users use the SHU coefficient as the first option to model $hmF2$ over Santa Maria, which is different from the recommendation of IRI-2016.

Data availability. The F10.7 index, sunspot number, and Kp index are publicly available on the following site: <https://omniweb.gsfc.nasa.gov/ow.html> (last access: 12 August 2019). The DPS data are available by contacting the responsible researcher at the CRCRS/COCRE/INPE-MCTIC (Juliano Moro, email: juliano.moro@inpe.br/julianopmoro@gmail.com).

Author contributions. JM conceived the study, processed the DPS data, designed the data analysis, and lead the writing of this paper. JX, CMD, LCAR, RPS, SSC, GAdSP, LZ, HL, CY, CW, and NJS assisted in the review of the paper and discussed the results of the study.

Competing interests. The authors declare that they have no conflict of interest.

Special issue statement. This article is part of the special issue “7th Brazilian meeting on space geophysics and aeronomy”. It is a result of the Brazilian meeting on Space Geophysics and Aeronomy, Santa Maria/RS, Brazil, 5–9 November 2018.

Acknowledgements. Juliano Moro would like to acknowledge the China-Brazil Joint Laboratory for Space Weather (CBJLSW), National Space Science Center (NSSC), and Chinese Academy of Sciences (CAS) for supporting his postdoctoral fellowship, and the National Council for Scientific and Technological Development (CNPq) for the grant 429517/2018-01. Clezio Marcos Denardini thanks CNPq for the fellowship under grant number 303643/2017-0. Laysa Cristina Araújo Resende would like to acknowledge the CBJLSW for supporting her postdoctoral fellowship. Régia Pereira Silva acknowledges the support from CNPq for grant number 300329/2019-9. Sony Su Chen thanks the Coordination for the Improvement of Higher Education Personnel (CAPES) for supporting his PhD. (grant number 88887.362982/2019-00). Giorgio Arlan da Silva Picanço thanks CAPES (grant 88887.351778/2019-00). Nelson Jorge Schuch thanks CNPq for the fellowship under grant number 300886/2016-0. The authors also thank OMNIWEB (<https://omniweb.gsfc.nasa>).

gov/form/dx1.html, last access: 12 August 2019) for providing the F10.7 index, sunspot number, and Kp index used in the classification of the days. The digisonde data from Santa Maria can be downloaded upon registration at the Embrace web page from INPE Space Weather Program at the following link: <http://www2.inpe.br/climaespacial/portal/en/> (last access: 5 August 2019). The authors acknowledge the support of the Federal University of Santa Maria (UFSM) Central Administration.

Financial support. This research has been supported by the CB-JLSW/NSSC/CAS and the National Council for Scientific and Technological Development – CNPq (grant no. 429517/2018-01).

Review statement. This paper was edited by Fabiano Rodrigues and reviewed by two anonymous referees.

References

- Abdu, M. A. and Brum, C. G. M.: Electrodynamics of the vertical coupling processes in the atmosphere-ionosphere system of the low latitude region, *Earth Planet. Space*, 61, 385–395, 2009.
- Altadill, D., Magdaleno, S., Torta, J. M., and Blanch, E.: Global empirical models of the density peak height and of the equivalent scale height for quiet conditions, *Adv. Space Res.*, 52, 1756–1769, 2013.
- Araujo-Pradere, E. A., Fuller-Rowell, T. J., and Codrescu, M. V.: Storm: an empirical storm-time ionospheric correction model – 1, Model description, *Radio Sci.*, 37, 1–12, 2002.
- Batista, I. S. and Abdu, M. A.: Ionospheric variability at Brazilian low and equatorial latitudes: comparison between observation and IRI model, *Adv. Space Res.*, 34, 1894–1900, 2004.
- Bertoni, F., Sahai, Y., Lima, W. L. C., Fagundes, P. R., Pilat, V. G., Becker-Guedes, F., and Abalde, J. R.: IRI-2001 model predictions compared with ionospheric data observed at Brazilian low latitude stations, *Ann. Geophys.*, 24, 2191–2200, <https://doi.org/10.5194/angeo-24-2191-2006>, 2006.
- Bilitza, D.: International Reference Ionosphere 1990, National Space Science Data Center, Report 90-22, Greenbelt, Maryland, USA, 1990.
- Bilitza, D.: International Reference Ionosphere 2000, *Radio Sci.*, 36, 261–275, 2001.
- Bilitza, D. and Rawer, K.: International Reference Ionosphere, in: *The Upper Atmosphere – Data Analysis and Interpretation*. Springer-Verlag, Berlin, Heidelberg, 735–772, 1996.
- Bilitza, D. and Reinisch, B.: International Reference Ionosphere 2007: Improvements and new parameters, *Adv. Space Res.*, 42, 4, 599–609, <https://doi.org/10.1016/j.asr.2007.07.048>, 2008.
- Bilitza, D., Sheikh, N. M., and Eyfrig, R.: A global model for the height of the F2-peak using M3000 values from the CCIR numerical map, *Telecommun. J.*, 46, 549–553, 1979.
- Bilitza, D., Altadill, D., Zhang, Y., Mertens, C., Truhlik, V., Richards, P., McKinnell, L.-A., and Reinisch, B.: The International Reference Ionosphere 2012 – a model of international collaboration, *J. Space Weather Spac.*, 4, 1–12, <https://doi.org/10.1051/swsc/2014004>, 2014.
- Bilitza, D., Altadill, D., Truhlik, V., Shubin, V., Galkin, I., Reinisch, B., and Huang, X.: International Reference Ionosphere 2016: From ionospheric climate to real-time weather predictions, *Adv. Space Res.*, 15, 418–429, <https://doi.org/10.1002/2016SW001593>, 2017.
- CCIR: Consultative Committee on International Radio, Atlas of ionospheric characteristics Report 340, International telecommunication Union, Geneva, Switzerland, 1967.
- CCIR: Atlas of Ionospheric Characteristics. Union Internationale des Télécommunications, Geneva, Report 340, 1–391, 1973.
- Denardini, C. M., Dasso, S., and Gonzalez-Esparza, J. A.: Review on space weather in Latin America, 3. Development of space weather forecasting centers, *Adv. Space Res.*, 58, 1960–1967, <https://doi.org/10.1016/j.asr.2016.03.011>, 2016.
- Ezquer, R. G., Mosert, M., Scida, L., and López, J.: Peak characteristics of F2 region over Tucumán: predictions and measurements, *J. Atmos. Sol.-Terr. Phys.*, 70, 1525–1532, 2008.
- Fuller-Rowell, T. J., Codrescu, M. C., and Wilkinson, P.: Quantitative modeling of the ionospheric response to geomagnetic activity, *Ann. Geophys.*, 18, 766–781, <https://doi.org/10.1007/s00585-000-0766-7>, 2000.
- Heirtzler, J.: The future of the South Atlantic anomaly and implications for radiation damage in space, *J. Atmos. Sol.-Terr. Phys.*, 64, 1701–1708, [https://doi.org/10.1016/S1364-6826\(02\)00120-7](https://doi.org/10.1016/S1364-6826(02)00120-7), 2002.
- Horne, R. B., Glauert, S. A., Meredith, N. P., Boscher, D., Maget, V., Heynderickx, D., and Pitchford, D.: Space weather impacts on satellites and forecasting the Earth’s electron radiation belts with SPACECAST, *Adv. Space Res.*, 11, 169–186, <https://doi.org/10.1002/swe.20023>, 2013.
- Jones, A. D., Kanekal, S. G., Baker, D. N., Klecker, B., Looper, M. D., Mazur, J. E., and Schiller, Q.: SAMPEX observations of the South Atlantic anomaly secular drift during solar cycles 22–24, *Adv. Space Res.*, 15, 44–52, <https://doi.org/10.1002/2016SW001525>, 2017.
- Kouris, S. S. and Muggleton, L. M.: Diurnal variation in the E-layer ionization, *J. Atmos. Sol.-Terr. Phys.*, 35, 133–139, 1973a.
- Kouris, S. S. and Muggleton, L. M.: World morphology of the Appleton E-layer seasonal anomaly, *J. Atmos. Sol.-Terr. Phys.*, 35, 141–151, 1973b.
- Liu, Z., Hanxian, F., Weng, L., Wang, S., Niu, J., and Meng, X.: A comparison of ionosonde measured foF2 and IRI-2016 predictions over China, *Adv. Space Res.*, 63, 1926–1936, <https://doi.org/10.1016/j.asr.2019.01.017>, 2019.
- Maltseva, O. A. and Poltavsky, O. S.: Evaluation of the IRI model for the European region, *Adv. Space Res.*, 43, 1638–1643, 2009.
- Moro, J., Denardini, C. M., Abdu, M. A., Correia, E., Schuch, N. J., and Makita, K.: Latitudinal dependence of cosmic noise absorption in the ionosphere over the SAMA region during the September 2008 magnetic storm, *J. Geophys. Res.*, 117, A06311, <https://doi.org/10.1029/2011JA017405>, 2012.
- Moro, J., Denardini, C. M., Abdu, M. A., Correia, E., Schuch, N. J., and Makita, K.: Correlation between the cosmic noise absorption calculated from the SARINET data and energetic particles measured by MEPED: Simultaneous observations over SAMA region, *Adv. Space Res.*, 51, 11692–1700, 2013.
- Moro, J., Denardini, C. M., Resende, L. C. A., Chen, S. S., and Schuch, N. J.: Influence of uncertainties of the empirical models for inferring the E-region electric fields at the dip equator, *Earth*

- Planet. Space, 68, 103–118, <https://doi.org/10.1186/s40623-016-0479-0>, 2016.
- Moro, J. M., Xu, J., Denardini, C. M., Resende, L. C. A., Silva, R. P., Liu, Z., Li, H., Yan, C., Wang, C., and Schuch, N. J.: On the sources of the ionospheric variability in the South American Magnetic Anomaly during solar minimum, *J. Geophys. Res.-Space*, 124, 7638–7653, <https://doi.org/10.1029/2019JA026780>, 2019.
- OMNIWeb (NASA): F10.7 index, sunspot number, and Kp index, available at: <https://omniweb.gsfc.nasa.gov/ow.html>, last access: 12 August 2019.
- Oyekola, O. S. and Fagundes, P. R.: Equatorial F2-layer variations: comparison between F2 peak parameters at Ouagadougou with the IRI-2007 model, *Earth Planet. Space*, 64, 553–566, 2012.
- Rawer, K., Bilitza, D., and Ramakrishnan, S.: International Reference Ionosphere, International Union of Radio Science (URSI), Brussels, Belgium, 1978a.
- Rawer, K., Bilitza, D., and Ramakrishnan, S.: Intensions and buildup of the International Reference Ionosphere, in: Operational Modeling of the Aerospace Propagation Environment, AGARD Conf. Proc., 238, 6.1–6.10, 1978b.
- Rawer, H., Lincoln, J. V., and Conkright, R. O.: International Reference Ionosphere – IRI 79, World Data Center for Solar-Terrestrial Physics, Report UAG-82, Boulder, Colorado, 1981.
- Rawer, K. and Bilitza, D.: International Reference Ionosphere-plasma densities: Status 1988, *Adv. Space Res.*, 10, 5–14, 1990.
- Rush C., Fox, M., Bilitza, D., Davies, K., McNamara, L., Stewart, F., and PoKempner, M.: Ionospheric mapping – an update of foF2 coefficients, *Telecomm. J.*, 56, 179–182, 1989.
- Schuch, N. J., Durão, O. S. C., da Silva, M. R., Mattiello-Francisco, F., Martins, J. B. S., Legg, A., da Silva, A., and Bürguer, E.: The NANOSATC-BR, Cubesat Development Program – a joint Cubesat Program developed by UFSM and INPE/MCTIC – Space geophysics mission payloads and first results, *Braz. J. Geophys.*, 37, 95–103, <https://doi.org/10.22564/rbgf.v37i1.1992>, 2019.
- Shubin, V. N.: Global median model of the F2-layer peak height based on ionospheric radio-occultation and ground-based Digisonde observations, *Adv. Space Res.*, 56, 916–928, 2015.
- Wang, C.: New Chains of Space Weather Monitoring Stations in China, *Adv. Space Res.*, 8, S08001, <https://doi.org/10.1029/2010SW000603>, 2010.
- Zhao, X., Ning, B., Zhang, M. L., and Hu, L.: Comparison of the ionospheric F2 peak height between ionosonde measurements and IRI2016 predictions over China, *Adv. Space Res.*, 60, 1524–1531, <https://doi.org/10.1016/j.asr.2017.06.056>, 2017.